

Multiplexed Fluorescence Unmixing

Marina Alterman , Yoav Y. Schechner
 Department of Electrical Engineering
 Technion - Israel Inst. Technology,
 Haifa 32000, Israel

amarina@tx.technion.ac.il, yoav@ee.technion.ac.il

Aryeh Weiss
 School of Engineering
 Bar-Ilan University,
 Ramat Gan 52900, Israel

aryeh@cc.huji.ac.il

Abstract

Multiplexed imaging and illumination have been used to recover enhanced arrays of intensity or spectral reflectance samples, per pixel. However, these arrays are often not the ultimate goal of a system, since the intensity is a result of underlying object characteristics, which interest the user. For example, spectral reflectance, emission or absorption distributions stem from an underlying mixture of materials. Therefore, systems try to infer concentrations of these underlying mixed components. Thus, computational analysis does not end with recovery of intensity (or equivalent) arrays. Inversion of mixtures, termed unmixing, is central to many problems. We incorporate the mixing/unmixing process explicitly into the optimization of multiplexing codes. This way, optimal recovery of the underlying components (materials) is directly sought. Without this integrated approach, multiplexing can even degrade the unmixing result. Moreover, by directly defining the goal of data acquisition to be recovery of components (materials) rather than of intensity arrays, the acquisition becomes more efficient. This yields significant generalizations of multiplexing theory. We apply this approach to fluorescence imaging.

1. Introduction

Images with poor signal-to-noise ratio (SNR) suffer from loss of high-frequency details (with high probability), as was recently quantified [36]. An increase in the SNR of intensity data arrays – without an increase in acquisition resources such as time – can be achieved using multiplexed sensing [11]. Therefore, multiplexing is used in multi-spectral imaging (array of spectral bands) [3, 10, 25, 31], spectroscopy [21, 35] and lighting (reflection from an array of light sources) [5, 20, 22, 28, 29, 32, 33, 37]. It also has analogous formulations in coded apertures and shuttering [1, 15, 16, 27]. The acquired multiplexed measurements are demultiplexed by a computer, yielding an array of intensity values with a higher SNR.

However, is a demultiplexed array the true goal of a vision system? Often not. Usually, the recovered intensity or reflectance array is an input to further analysis (see [24]).

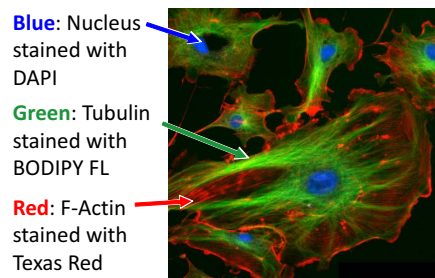


Figure 1. Cells rendered for color display, by associating each of the RGB channels with fluorescent emission by a specific dye. Each dye is excited by different spectral bands. Each dye is attached to a distinct component of the cells. Rendered image taken from the ImageJ sample collection [26].

For example, a multispectral imager may recover a scene's spectral datacube, and multiplexing is helpful in this. But the resulting multispectral datacube itself is of little interest *per se*: usually (e.g., in remote sensing) the user is interested in the underlying spatial distribution of *materials* or objects that created the spectral data. The end product of interest in this example is *not* demultiplexed intensities or spectral reflectance, but a distribution of materials. Similarly, in multispectral imaging of fluorescing specimens (as displayed in Fig. 1), intensities are just a means to obtain information about molecular distributions in the specimens. This occurs in other domains: multiplexed lighting [28, 32] improves single-source images, but often single-source images are further analyzed e.g., by photometric stereo.

Multiplexing has mostly been considered as an “SNR improvement black box,” distinct from the consequent vision task. Multiplexing codes have largely been optimized irrespective of the underlying core information, which is *not* an array of intensities or reflectance.

This paper is concerned explicitly with the task of unveiling the underlying variables of interest. The paper shows that this task should (and can) be fully integrated when optimizing the multiplexing codes. Otherwise, the true underlying variables of interest may not benefit properly from multiplexing, and may even *be harmed* by it. This detrimental effect is interesting, in that it shows that an optimized quality of a recovered intensity array does not guarantee su-

perior performance in the eventual task. Furthermore, an integrated optimization approach makes acquisition more *efficient*, since the underlying unknown variables usually have a lower dimension than the intermediate intensity array.

We thus develop a theory for multiplexed sensing, in which the end task is linear unmixing. Unmixing inverts natural cross-talk effects, such as blur and spectral mixtures. We focus on fluorescent imaging, in which the image formation model is more elaborate than reflection, and provides ample modeling challenges, cross-talk effects, highly non-uniform objects, and noise. We generalize the theory of multiplexing to deal with these challenging effects and task. This has useful applications in the life sciences, where fluorescence microscopy is a powerful tool. Furthermore, microscopic fluorescing specimens are often dim, and thus should truly benefit from any SNR improvement.

2. Theoretical Background

We study *unmixing* improvement using *multiplexed* acquisition, particularly in *fluorescence*. We now give background on these respective topics.

2.1. Fluorescence and Unmixing

A fluorescent dye (fluorophore) can attach to molecules in specific cell organelles. This labels the organelles, which can then be observed in high contrast to their surroundings (Fig. 1). Under irradiance from a source, the molecules absorb light and become *excited*. Their return to the ground energy state is accompanied by *emission* of light [12] (see Fig. 2) at a distinct spectrum. The emitted light is captured by a camera, yielding a digital output graylevel i .

Since different fluorescent dyes label different molecules and organelles, it is important to distinguish between them when analyzing fluorescent images. The distinction between dyes is hampered by an overlap in their excitation spectra. For example, Fig. 3[Top] shows the overlap in excitation spectra of the dyes *Alexa Fluor 488* (AF-488) and *MitoTracker Orange*. Using an excitation wavelength $\lambda^{\text{ex}} = 500\text{nm}$ would strongly excite AF-488, but excite MitoTracker Orange as well.

A similar situation is seen in Fig. 3[Bottom] with respect to emission. Sensing the emission at $\lambda^{\text{em}} = 540\text{nm}$ would spot both dyes, although AF-488 is more dominant. The overlap between the absorption spectra of various dyes, in addition to the overlap between their emission spectra yields *cross-talk* [39]. This is a fundamental problem [39] in visualization, analysis and quantification. Thus, image acquisition must be followed by an *unmixing* procedure.

The imaging setup (usually a microscope) has N_{sources} illumination sources. It also has N_{filter} channels (or filters) that pass different fluorescence emission bands to the sensor. Let $s \in [1, N_{\text{sources}}]$ index the excitation source, $d \in [1, N_{\text{dyes}}]$ index the fluorescent dye, and $f \in [1, N_{\text{filter}}]$ index the fluorescence emission channel filter. Without loss

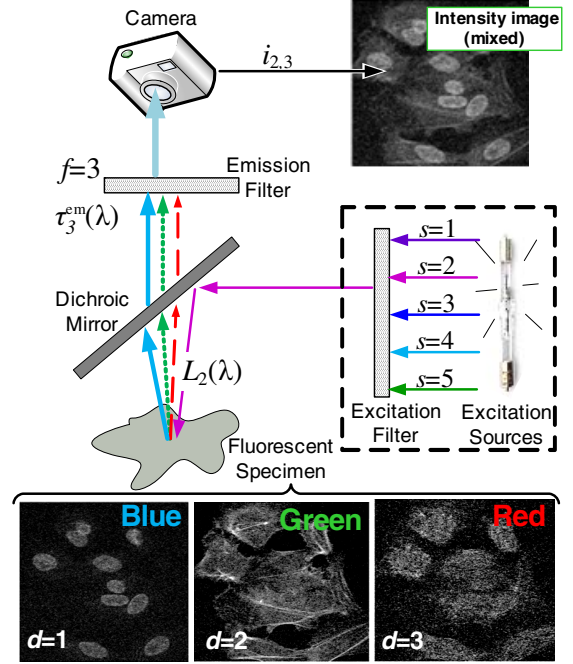


Figure 2. *Fluorescence process and mixing.* In this example, a specimen has three dyes. Source $s = 2$ (violet light) with irradiance $L_2(\lambda)$ excites mostly dye $d = 1$, but also (more weakly) dyes $d = 2, 3$. In response, each dye emits a different spectrum. Dye $d = 1$ emits in blue. The other dyes also emit there (*crosstalk/mixing*), but more weakly. Emission filter $f = 3$ blocks all light (with the aid of a dichroic mirror), passing only the blue band associated with $d = 1$. This filter’s transmissivity is τ_3^{em} . Due to the crosstalk, the recorded image $i_{2,3}$ is affected also by light emitted by dye $d = 2$. The goal is to remove the crosstalk (*unmix*), and isolate each dye, i.e., view an image of its concentration c_d .

of generality, consider a common case, where the illumination (excitation) source is fixed (s is degenerate), while $N_{\text{filters}} \geq N_{\text{dyes}}$. A multispectral image is thus obtained. Corresponding to the set of emission bands, the intensities at any pixel form a vector $\mathbf{i} = (i_1, i_2, \dots, i_{N_{\text{filters}}})^T$, where T denotes transposition. Let c_d denote the molar concentration [$\text{M} \cdot \text{cm}^{-2}$] of fluorophore d at an area corresponding to a pixel. Concatenate the set $\{c_d\}_{d=1}^{N_{\text{dyes}}}$ to $\mathbf{c} = (c_1, c_2, \dots, c_{N_{\text{dyes}}})^T$. Then [34],

$$\mathbf{i} = \mathbf{X} \mathbf{c} . \quad (1)$$

Here \mathbf{X} is a *mixing matrix*. Image acquisition is not limited to this configuration. Alternatively, it can be based on modulating the excitation using N_{sources} different sources, while keeping f degenerate. Then, Eq. (1) also holds, but its elements are different. In any case, the matrix \mathbf{X} is *known*,¹ for a given acquisition system and a given set of dyes, as we describe later in Sec. 7.

The role of *unmixing* [39] (or *separation*) is to invert the cross-talk in \mathbf{i} : decouple the components in \mathbf{c} , based on \mathbf{i} , across the image. If \mathbf{X} is invertible, unmixing is achieved by $\hat{\mathbf{c}} = \mathbf{X}^{-1} \mathbf{i}$.

¹When \mathbf{X} is unknown, this is a problem of blind source separation [23].

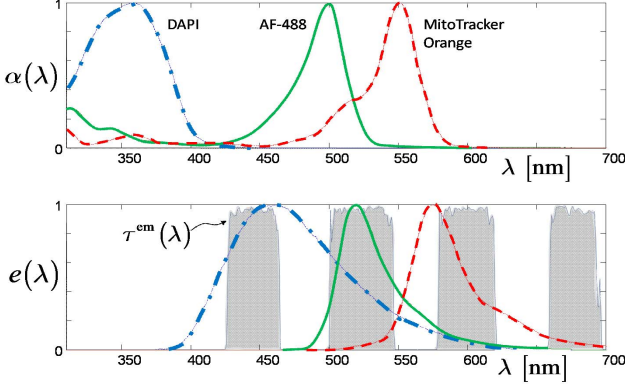


Figure 3. Absorption [Top] and emission [Bottom] spectra of three dyes [18], displayed peak-normalized. Overlaid is τ^{em} of the multiband filter described in Sec. 8.

2.2. Multiplexing

Often, sensors seek measurement of a vector of observable variables, such as \mathbf{i} . Nevertheless, the acquired raw measurements often form a vector \mathbf{a} of length N_{measure} . This raw vector is related to \mathbf{i} by

$$\mathbf{a} = \mathbf{W}\mathbf{i} + \eta, \quad (2)$$

where η is a vector of measurement noise (the noise is uncorrelated in different measurements). Here \mathbf{W} is a weighting matrix, referred to as a *multiplexing code*. One case is $\mathbf{W} = \mathbf{I}$, where \mathbf{I} is the identity matrix. This special case is referred to as *trivial* sensing: only a single component of \mathbf{i} is acquired at a time. More generally, multiple components of \mathbf{i} can be summed up (multiplexed) and acquired in each raw measurement. The components of \mathbf{i} included in the m 'th measurement are determined by the m 'th row of \mathbf{W} .

Often, the vector \mathbf{i} corresponds to a pixel in the field of view, under different imaging settings. In our context, we may set \mathbf{i} to correspond to the pixel values, when the specimen is irradiated by a set of different excitation sources (Eq. 1), where f is degenerate. In this case, multiplexing using a general \mathbf{W} means that the sample is irradiated by multiple excitation sources (bands) simultaneously [21, 31, 35].

The elements $w_{m,s} \in [0, 1]$ of \mathbf{W} represent [25, 28, 32] the normalized radiance of source s in measurement m . If $w_{m,s} = 0$, then excitation source s is turned off completely at measurement m ; if $w_{m,s} = 1$, then this excitation source irradiates the specimen at the source's maximum power.

When \mathbf{W} is invertible, the individual variables of interest can be reconstructed using

$$\hat{\mathbf{i}} = \mathbf{W}^{-1} \mathbf{a}. \quad (3)$$

The mean squared error (MSE) [11, 21, 27, 28, 32] of $\hat{\mathbf{i}}$ is

$$\text{MSE}_{\mathbf{i}} = \frac{\sigma^2}{N_{\text{sources}}} \text{tr} \left[(\mathbf{W}^T \mathbf{W})^{-1} \right], \quad (4)$$

where tr is a trace operation, and σ^2 is the variance of η . Using Eqs. (3,4), $\hat{\mathbf{i}}$ can be reconstructed with a potentially

$$\begin{array}{c} \text{acquired} \\ \text{measurements} \\ \left[\mathbf{a} \right] \\ N_{\text{measure}} \times 1 \end{array} = \begin{array}{c} \mathbf{W} \\ \text{multiplexing} \\ \text{matrix} \\ N_{\text{measure}} \times N_{\text{sources}} \end{array} \begin{array}{c} \mathbf{i} \\ N_{\text{sources}} \times 1 \\ \left[\mathbf{X} \right] \\ \text{mixing} \\ \text{matrix} \\ N_{\text{sources}} \times N_{\text{dyes}} \end{array} \begin{array}{c} \left[\mathbf{c} \right] \\ N_{\text{dyes}} \times 1 \end{array} + \begin{array}{c} \text{noise} \\ \left[\eta \right] \\ N_{\text{measure}} \times 1 \end{array}$$

Figure 4. The model, along with its matrices, vectors and dimensions

higher SNR [11, 28, 32] than \mathbf{i} that is *trivially*-sensed using \mathbf{I} . The *gain* of using multiplexing (termed *multiplex advantage*) is defined [11] as

$$\text{GAIN}_{\mathbf{i}} = \sqrt{\sigma^2 / \text{MSE}_{\mathbf{i}}}. \quad (5)$$

Most related studies have aimed to maximize the SNR of the recovered images $\hat{\mathbf{i}}$. Thus, Refs. [8, 11, 25, 28, 32] sought a multiplexing matrix that minimizes Eq. (4):

$$\hat{\mathbf{W}}_{\mathbf{i}} = \arg \min_{\mathbf{W}} \text{MSE}_{\mathbf{i}}, \quad \text{s.t. } 0 \leq w_{m,s} \leq 1. \quad (6)$$

This work studies a different problem. We are interested in *optimal reconstruction* of \mathbf{c} . We are *not* interested in \mathbf{i} *per se*. Thus, using the linear models of Eqs. (1,2), we seek codes \mathbf{W} that are specifically made to yield eventual unmixing of the highest quality in the sense of minimal MSE.

3. Multiplexed Unmixing

The analysis in this section holds regardless of the specific mixing mechanism, be it via modulated excitation, modulated emission, or by any other linear process that may occur in sensors, such as blur. A vector of interest \mathbf{c} is mixed by a natural process, expressed by \mathbf{X} . The outcome is a vector \mathbf{i} , each of whose elements corresponds to an active source. Let multiple sources be active in each measurement (intentional multiplexing). Using Eqs. (1,2), the vector of raw multiplexed measurements is

$$\mathbf{a} = \mathbf{W}\mathbf{X}\mathbf{c} + \eta. \quad (7)$$

The dimensions of all the matrices and vectors in Eq. (7) are illustrated in Fig. 4. Define

$$\mathbf{W}_{\mathbf{x}} \equiv \mathbf{W}\mathbf{X}, \quad (8)$$

whose elements are denoted by $w_{m,d}^{\mathbf{x}}$. Now, we wish to decode \mathbf{c} , based on \mathbf{a} .

What should $\{N_{\text{sources}}, N_{\text{measure}}\}$ be? Obviously, when $N_{\text{dyes}} > N_{\text{sources}} > N_{\text{measure}}$, both \mathbf{W} and $\mathbf{W}_{\mathbf{x}}$ are rank deficient, and thus neither \mathbf{i} nor \mathbf{c} are recoverable.² To recover \mathbf{c} , the minimal required number of measurements is $N_{\text{measure}} = N_{\text{dyes}}$. However, more excitation sources may be available in the system than the number of dyes

²Underdetermined systems can be solved by introducing priors. In compressed sensing, sparsity of the signal is used as a prior [10].

($N_{\text{sources}} \geq N_{\text{dyes}}$). Thus, generally, the multiplexing matrix \mathbf{W} is not square, as illustrated in Fig. 4. Let us examine some possibilities:

Case 1. $N_{\text{measure}} > N_{\text{sources}} > N_{\text{dyes}}$

Here both \mathbf{W} and \mathbf{W}_x are full-rank, enabling recovery of both \mathbf{i} and \mathbf{c} . This is not highly efficient, though, since there are more measurements than independent unknowns. The vector \mathbf{c} can be estimated, for example, by using weighted least squares (WLS). As in [7], let the least squares weighting matrix be $\Sigma_{\text{noise}}^{-1}$, where Σ_{noise} is the covariance matrix of the raw measurement noise η . Then,³

$$\hat{\mathbf{c}} = \left(\mathbf{W}_x^T \Sigma_{\text{noise}}^{-1} \mathbf{W}_x \right)^{-1} \mathbf{W}_x^T \Sigma_{\text{noise}}^{-1} \mathbf{a}. \quad (9)$$

The special subcase $N_{\text{measure}} = N_{\text{sources}}$ corresponds to classical demultiplexing [11] of \mathbf{i} .

Case 2. $N_{\text{sources}} > N_{\text{measure}} > N_{\text{dyes}}$

Demultiplexing \mathbf{i} is ill-posed, since $\text{rank}(\mathbf{W}) < N_{\text{sources}}$. Nevertheless, \mathbf{c} is recoverable using Eq. (9).

Case 3. $N_{\text{sources}} > N_{\text{measure}} = N_{\text{dyes}}$

Here \mathbf{c} is recoverable, using *efficient acquisition* (the number of measurements matches the number of unknowns). Thus this case is of highest interest. It is tailored to recover \mathbf{c} . Here \mathbf{W}_x is square; thus (9) degenerates to $\hat{\mathbf{c}} = \mathbf{W}_x^{-1} \mathbf{a}$. Demultiplexing \mathbf{i} is ill-posed, as $\text{rank}(\mathbf{W}) < N_{\text{sources}}$.

Case 4. $N_{\text{sources}} = N_{\text{measure}} = N_{\text{dyes}}$

As in Case 1, \mathbf{i} and \mathbf{c} are recoverable. As in Case 3, the acquisition is *efficient*: the number of measurements matches N_{dyes} . It is tailored to recover \mathbf{c} , but exploits fewer sources than Case 3. Hence Case 4 provides *less flexibility*, leading to worse codes \mathbf{W} than in Case 3. Case 4 is useful when hardware (or monetary) constraints force mounting and using the least number of sources.

4. Optimal Multiplexing for Unmixing

We wish to multiplex measurements in a way that the recovered \mathbf{c} would be optimally recovered in the sense of minimal MSE. Hence, we need a multiplexing matrix \mathbf{W} that minimizes the MSE of \mathbf{c} ,

$$\widehat{\mathbf{W}}_{\mathbf{c}} = \arg \min_{\mathbf{W}} \text{MSE}_{\mathbf{c}}, \quad \text{s.t.} \quad 0 \leq w_{m,s} \leq 1. \quad (10)$$

In the following, we derive $\text{MSE}_{\mathbf{c}}$ when the estimator⁴ is Eq. (9). The noise in Eq. (7) propagates to $\hat{\mathbf{c}}$. The covariance matrix of $\hat{\mathbf{c}}$ is

$$\Sigma = \text{E} [(\hat{\mathbf{c}} - \mathbf{c})(\hat{\mathbf{c}} - \mathbf{c})^T] = \left(\mathbf{W}_x^T \Sigma_{\text{noise}}^{-1} \mathbf{W}_x \right)^{-1}, \quad (11)$$

where E denoted expectations. Thus,

³WLS optimizes fitting to the model (Eq.7), even when the noise variance changes between measurements (not identically distributed), as occurs in photon noise. The fit is optimal only for Gaussian noise. Photon noise is Poissonian, but it is well-approximated as Gaussian [32], when the expected number of photoelectrons per pixel is larger than 10.

⁴The WLS estimator does not minimize $\text{MSE}_{\mathbf{c}}$ for a given \mathbf{W}_x . There are more sophisticated estimators, which also incorporate priors on \mathbf{c} , such as non-negativity. Using such estimators can improve $\widehat{\mathbf{W}}_{\mathbf{c}}$ as well as $\hat{\mathbf{c}}$.

$$\text{MSE}_{\mathbf{c}} = \frac{1}{N_{\text{dyes}}} \text{tr} \left[\left(\mathbf{W}_x^T \Sigma_{\text{noise}}^{-1} \mathbf{W}_x \right)^{-1} \right]. \quad (12)$$

Let us look more closely at Σ_{noise} . Since the noise is independent in different measurements, Σ_{noise} is diagonal [8]. Each value at the diagonal is the variance σ_m^2 of the corresponding measurement m . With noise caused during detection [8, 21, 27, 28, 32, 38], the graylevel noise variance in a measurement can be expressed [13, 32] as

$$\sigma_m^2 \approx \sigma_{\text{gray}}^2 + a_m / g_{\text{gray}}^{\text{cam}}, \quad (13)$$

where σ_{gray}^2 is the variance of the signal-independent noise components (read-out, dark current and quantization) and $g_{\text{gray}}^{\text{cam}}$ is the number of photoelectrons required to change a unit graylevel of the camera. The second component in Eq. (13) is signal-dependent, and is referred to as photon or shot noise. Using the elements a_m from Eq. (7) in Eq. (13),

$$\sigma_m^2 \approx \sigma_{\text{gray}}^2 + \sum_{d=1}^{N_{\text{dyes}}} w_{m,d}^x \nu_d^2, \quad (14)$$

where $\nu_d^2 = c_d / g_{\text{cam}}^{\text{gray}}$ is the photon noise variance induced by dye d in the specimen if $w_{m,d}^x = 1$. As such, ν_d^2 and σ_m^2 are specimen-dependent.

Our cost function (Eq. 12) is more complicated and generalized than in previous works [16, 21, 27, 28, 32], for two reasons. First, *natural* mixing \mathbf{X} is incorporated into the cost function, in addition to the intentionally *man-made* multiplexing (\mathbf{W}), through (8). Second, Σ_{noise} is incorporated into the core of the cost function, and it is *not* trivially factored out, contrary to much of the prior work. Assume for a moment that the noise variance (Eq. 14) is brightness-independent, i.e., $\sigma_m^2 \approx \sigma^2, \forall m$. Then, $\Sigma_{\text{noise}} = \sigma^2 \mathbf{I}$, degenerating (12) simply to $\text{MSE}_{\mathbf{c}} \propto \sigma^2 \text{tr} [(\mathbf{W}_x^T \mathbf{W}_x)^{-1}]$. Similarly, such a simple form is used in Eq. (4) and also when accounting for photon noise in Ref. [28]. Why don't we use this simplified form here?

The reason is that photon noise may vary significantly between dyes, in typical specimens. See, for example, Fig. 2. Overall, much more light is emitted by dye $d=1$ than by $d=2$. Thus, should multiplexing increase the emission from $d=1$, the overall photon noise and thus the penalty to $\text{MSE}_{\mathbf{c}}$ may increase substantially. So, optimized multiplexing may avoid an increase of emission from $d=1$. Instead, it may increase the emission from $d=2$. This balancing of emissions is taken care of, by using the generalized cost function (Eq. 12), with a nonuniform diagonal in Σ_{noise} .

To solve Eq. (10), we use the projected gradient descent method [4]: $\text{MSE}_{\mathbf{c}}$ is iteratively minimized as a function of \mathbf{W} in accordance with Ref. [28], as detailed in [2].

5. Generalized Multiplex Gain

When using the matrix $\widehat{\mathbf{W}}_{\mathbf{c}}$ derived by Eq. (10), what is the SNR gain in the recovery of \mathbf{c} ? In past studies, gain has been defined as the SNR change, relative to *trivial* sensing ($\mathbf{W} = \mathbf{I}$). This definition leads to Eq. (5), for instance.

Analogously to [28], the multiplex SNR gain of \hat{c} is thus

$$\text{GAIN}_c = \sqrt{\text{MSE}_c^{\text{triv}} / \text{MSE}_c}, \quad (15)$$

where $\text{MSE}_c^{\text{triv}}$ is the MSE of \hat{c} obtained when only a single excitation source is operated at a time. This principle is simple to apply when \mathbf{W} is square, specifically in Case 4 (Sec. 3). Here, using $\mathbf{W} = \mathbf{I}$ in Eqs. (8,12) yields

$$\text{MSE}_c^{\text{triv}} = \frac{1}{N_{\text{dyes}}} \text{tr} \left[(\mathbf{X}^T \boldsymbol{\Sigma}_{\text{noise}}^{-1} \mathbf{X})^{-1} \right]. \quad (16)$$

However, defining $\text{MSE}_c^{\text{triv}}$ is not “trivial” when \mathbf{W} is not square, as in the important Case 3 described in Sec. 3. In this case, there are N_{sources} sources, but we do not have the opportunity to use all of them, one by one, within the fewer measurements ($N_{\text{measure}} < N_{\text{sources}}$). Which ones should we use in single-source illumination, and which should be discarded? The choice affects MSE_c under this illumination and thus should be made with care.

Let Ω be the set of all available excitation sources, where $|\Omega| = N_{\text{sources}}$. A subset of excitation sources actually used is $\tilde{\Omega} \subseteq \Omega$, where $|\tilde{\Omega}| = N_{\text{measure}}$. This subset of sources defines a mixing matrix $\tilde{\mathbf{X}}(\tilde{\Omega})$, whose N_{measure} rows are a subset of the rows of \mathbf{X} , corresponding to the sources in $\tilde{\Omega}$. Using $\tilde{\mathbf{X}}(\tilde{\Omega})$ instead of \mathbf{X} in Eq. (16) yields a value $\text{MSE}_c^{\text{triv}}[\tilde{\mathbf{X}}(\tilde{\Omega})]$. For best “trivial” sensing, we seek the optimal subset. It is found by optimization:

$$\tilde{\Omega} = \arg \min_{\tilde{\Omega} \subseteq \Omega} \{ \text{MSE}_c^{\text{triv}}[\tilde{\mathbf{X}}(\tilde{\Omega})] \}. \quad (17)$$

The gain is then defined as

$$\text{GAIN}_c = \sqrt{\{ \text{MSE}_c^{\text{triv}}[\tilde{\mathbf{X}}(\tilde{\Omega})] \} / \text{MSE}_c}. \quad (18)$$

For example, suppose we want to unmix three dyes, using $N_{\text{measure}} = 3$ frames. The setup has $N_{\text{sources}} = 5$ available illumination (excitation) sources. For optimal multiplexed unmixing, *all five sources* are used, as described in Secs. 3 and 4, yielding an optimal MSE_c . The gain achieved by this multiplexing is assessed using Eq. (18). Towards this, potential subsets $\tilde{\Omega}$ would be $\{s = 1, 2, 5\}$, $\{s = 2, 3, 5\}$, etc. The matrix $\tilde{\mathbf{X}}(\{s = 1, 3, 4\})$ is made of rows 1,3, and 4 of \mathbf{X} . If this subset happens to yield the minimum in Eq. (17), then it is used in Eq. (18).

6. Performance Bounds

The gain has lower and upper bounds. The recovery MSE (Eq. 12) depends on the raw image noise (Eq. 13). The latter depends on the distribution of dyes in the specimen (Eq. 14) and the system characteristics.

Suppose light added by multiplexed excitation of dyes does not effectively increase the raw noise, at any pixel. This is the case when photon noise is negligible, i.e., when $\sigma_{\text{gray}}^2 \gg a_m / g_{\text{gray}}^{\text{cam}} \forall m$, e.g, at dim specimens, or when using cameras having high readout or dark-current noise.

It may also occur in spatially very sparse specimens, where different dyes do not overlap spatially. When increased photon noise is not a major inhibitor, multiplexing exploits its potential [11, 28, 38], yielding the *upper bound* of gain.

The opposite occurs when photon noise dominates the entire specimen, while multiplexing significantly increases the noise everywhere. This occurs in uniform, bright specimens, i.e. a blank sample with high density of dyes, smeared uniformly without any spatial variations. Adding active sources by multiplexing increases photon noise in all raw pixels, inhibiting the method and yielding the *lower bound* of gain. Fortunately, such uniform specimens are of no interest to users. Typical fluorescing samples are rather sparse (Figs. 1,2). Thus, GAIN_c lies well between the bounds.

7. What is \mathbf{X} ?

This section describes how the elements of \mathbf{X} are formulated for fluorescence. The pixel graylevel depends linearly⁵ on the following factors [9, 19]:

- $L_s(\lambda)$ [photons · sec⁻¹cm⁻²nm⁻¹], spectral intensity distribution of excitation source s .
- ε_d [M⁻¹ · cm⁻¹], molar extinction coefficient of fluorophore d . It represents the peak absorbance of the dye (at the wavelength yielding the strongest absorbance) [18].
- $\alpha_d(\lambda)$ [%], absorption spectrum of fluorophore d . It is peak-normalized, i.e., $\max[\alpha(\lambda)] = 1$.
- Φ_d [%], quantum yield for emission by excited fluorophore d . It represents the probability for photon emission by an excited molecule, over the entire emission spectrum.
- $e_d(\lambda)$ [%], normalized emission spectral distribution⁶ of fluorophore d , where $\int e_d(\lambda) d\lambda = 1$.
- t^{exp} [sec], exposure time.
- h [cm], thickness of the specimen.
- A^{pixel} [cm²], object area imaged by a camera pixel.
- $q_{\text{elect}}^{\text{cam}}(\lambda)$ [elect · photons⁻¹ · nm⁻¹], quantum efficiency of the detector, per unit wavelength.
- $\tau_f^{\text{em}}(\lambda)$ [%], transmissivity of the optics in the *emission* path of the imaging setup, when filter f is used. This number also encapsulates the setup’s numerical aperture.

Let N_{dyes} dyes be viewed through filter f and under excitation (illumination) source s . The pixel value [9] is then

$$i_{s,f} = \sum_{d=1}^{N_{\text{dyes}}} \frac{1}{g_{\text{gray}}^{\text{cam}}} t^{\text{exp}} h A^{\text{pixel}} \Phi_d \varepsilon_d c_d \cdot \int_{\lambda_{\text{em}}} \tau_f^{\text{em}}(\lambda) q_{\text{elect}}^{\text{cam}}(\lambda) e_d(\lambda) d\lambda \int_{\lambda_{\text{ex}}} L_s(\lambda) \alpha_d(\lambda) d\lambda. \quad (19)$$

⁵Scientific-grade cameras have a linear radiometric response. Nonlinear fluorescence can be caused by secondary absorption of emitted light in very high fluorophore concentrations, or by two-photon microscopy, which requires special, very high intensity pulsed lasers.

⁶The emitted spectral distribution is insensitive to the energy of the exciting photons. Therefore, different excitation wavelengths result in different emission intensities, but similar spectral distributions [19].

7.1. Modulating Excitation and Emission

The formulations in this paper hold regardless of the switching mechanism of s and f . However, for completeness, we outline some implementations. Modulating (turning on/off) the emission bands: [i] Filter set; [ii] Acousto-optical tunable filter (AOTF); [iii] Dispersion. Option [iii] easily yields a large N_{filter} in scanning optics, but it is more challenging to implement in widefield setups [10]. In widefield, options [i,ii] require large aperture components. Thus, *excitation modulation* and multiplexing (s changes, while f is degenerate) are easier to use in widefield imaging.

Modulating the excitation spectrum $L_s(\lambda)$: [a] Multiple lasers shined via an AOTF; [b] Arc lamp shined via a filter set or an AOTF; [c] Arc lamp dispersion via a prism or grating, into a spatial light modulator (e.g., LCD); [d] A tree of multiple coaxial light emitting diodes (LEDs) [6], each of a narrow waveband. It is easy to modulate the intensity of LEDs and multiplex them. They can work with common (simple) widefield microscopes.

7.2. Excitation Modulation

For unmixing purposes, it is sufficient to estimate the concentrations $\{c_d\}_{d=1}^{N_{\text{dyes}}}$ up to a global constant, which is independent of the dye and spatial location. Let us define a dye-independent system characteristic κ^{sys} and a globally-scaled vector of concentrations

$$\tilde{\mathbf{c}} \equiv \kappa^{\text{sys}} \mathbf{c}, \quad (20)$$

whose elements are denoted by \tilde{c}_d . Estimating the concentrations up to a global scale has a practical benefit: the system does not need to be absolutely calibrated: only unit-less *relative* curves of $L_s(\lambda)$ etc. need to be known. For relative expressions, define the peak spectral irradiance among all sources $L_{\text{max}} = \max_{\lambda,s} L_s(\lambda)$, the peak optical transmissivity among all emission channels/filter $\tau_{\text{max}}^{\text{em}} = \max_{\lambda,f} \tau_f^{\text{em}}(\lambda)$, and the peak quantum efficiency $q_{\text{max}}^{\text{cam}} = \max_{\lambda} q_{\text{elect}}^{\text{cam}}(\lambda)$. Normalizing $L_s(\lambda)$, $\tau_f^{\text{em}}(\lambda)$ and $q_{\text{elect}}^{\text{cam}}(\lambda)$ by these respective constants yields the *relative* spectral distributions $\tilde{L}_s(\lambda)$, $\tilde{\tau}_f^{\text{em}}(\lambda)$ and $\tilde{q}_{\text{elect}}^{\text{cam}}(\lambda)$. Then the dye-independent system constant in Eq. (20) is

$$\kappa^{\text{sys}} \equiv t^{\text{exp}} h A^{\text{pixel}} L_{\text{max}} \tau_{\text{max}}^{\text{em}} q_{\text{max}}^{\text{cam}} / g_{\text{gray}}^{\text{cam}}. \quad (21)$$

When f is degenerate, Eqs. (19,20,21) yield

$$i_s = \sum_{d=1}^{N_{\text{dyes}}} \Phi_d \varepsilon_d \tilde{c}_d \cdot \int_{\lambda^{\text{em}}} \tilde{\tau}^{\text{em}}(\lambda) \tilde{q}_{\text{elect}}^{\text{cam}}(\lambda) e_d(\lambda) d\lambda \int_{\lambda^{\text{ex}}} \tilde{L}_s(\lambda) \alpha_d(\lambda) d\lambda. \quad (22)$$

Eq. (22) can be written in a vector form as in Eq. (1), where $\tilde{\mathbf{c}}$ replaces \mathbf{c} . Here, \mathbf{X} is a *mixing matrix* of size $N_{\text{sources}} \times N_{\text{dyes}}$ whose elements are

$$x_{s,d} = \Phi_d \varepsilon_d \int_{\lambda^{\text{em}}} \tilde{\tau}^{\text{em}}(\lambda) \tilde{q}_{\text{elect}}^{\text{cam}}(\lambda) e_d(\lambda) d\lambda \int_{\lambda^{\text{ex}}} \tilde{L}_s(\lambda) \alpha_d(\lambda) d\lambda \quad (23)$$

Estimating $\tilde{\mathbf{c}}$ rather than \mathbf{c} does not change the optimization procedure we described.

Eq. (23) applies to modulating and multiplexing of excitation sources while f is degenerate (no emission multiplexing). This is a special case. The formulation applies just as well to modulating and multiplexing of emission channels. Moreover, *both* emission and excitation channels can be modulated *simultaneously* in \mathbf{X} and \mathbf{W} . These added degrees of freedom increase flexibility and the optimization domain. This is expected to increase gain.

8. Simulated Examples

Let a camera have $g_{\text{gray}}^{\text{cam}} = 50$ and $\sigma_{\text{gray}} = 0.5$, similarly to data given in [32], and an approximately uniform $\tilde{q}_{\text{elect}}^{\text{cam}}$. The camera is mounted with a fixed *Semrock LF405/488/561/635 Quad Emission Filter* (where f is degenerate), which has multiple passbands. Its transmissivity $\tilde{\tau}^{\text{em}}(\lambda)$ is plotted in Fig. 3. The specimens in the following examples all have $N_{\text{dyes}} = 3$. The dye sets are

$$\mathcal{D}_1 = \{\text{DAPI, AF-488, MitoTracker Orange}\}$$

$$\mathcal{D}_2 = \{\text{AF-488, AF-555, AF-633}\}$$

$$\mathcal{D}_3 = \{\text{ECFP, EYFP, mRFP1}\}.$$

Each dye represents a different cell organelle, such as nucleus, cytoskeleton and mitochondrion. The physical characteristics $\{\varepsilon_d, \alpha_d(\lambda), \Phi_d, e_d(\lambda)\}$ of each dye are listed in the literature [18]. For example, the spectra corresponding to \mathcal{D}_1 are plotted in Fig. 3, where dye cross-talk is well apparent. The excitation wavelengths λ^{ex} are all in the stop-bands of $\tilde{\tau}^{\text{em}}(\lambda)$, to block them from the camera. All the source distributions $\{\tilde{L}_s(\lambda^{\text{ex}})\}_{s=1}^{N_{\text{sources}}}$ are set to have the same peak intensity.

Gain Within Performance Bounds

First, for \mathcal{D}_1 , we obtain the gain's *upper bound* and *lower bound*, using *efficient* acquisition, i.e., $N_{\text{measure}} = 3$. The bounds are defined by two specimens characterized in Sec. 6 as either dark or uniform, respectively.

For example, let $N_{\text{sources}} = 4$. Then, a set Ω of four narrow-band excitation sources was selected, all within the stop-bands of $\tilde{\tau}^{\text{em}}(\lambda)$. The set Ω affects \mathbf{X} and thus the resulting $\text{MSE}_{\mathbf{c}}$. Hence, it is selected by an optimization process. Eq. (10) was then solved for each of the two specimens.⁷ Using Eqs. (12,18), $\text{GAIN}_{\mathbf{c}}$ was derived. The same process was repeated for various values of N_{sources} . The resulting bounds are plotted in Fig. 5.

Next, we considered three specimens having realistic distributions: *Specimen-I* is shown in Fig. 2; *Specimen-II* has a few small cells and a large empty area; *specimen-III* has a large cell with little empty areas. The different distributions affect the optimization, as explained in Sec. 4. The gains corresponding to each are plotted in Fig. 5. All are indeed within the bounds. In

⁷The noise parameters were assessed as explained in App. A.

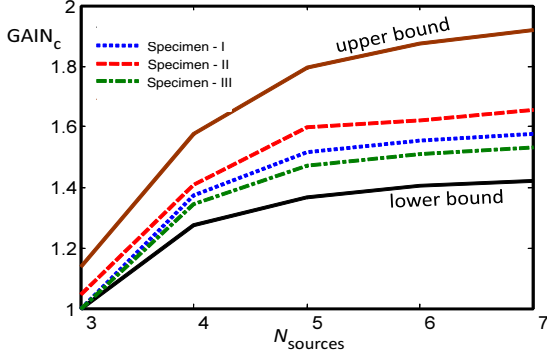


Figure 5. Unmixing gain for different specimens (thus different spatial distributions) of dye set \mathcal{D}_1 , under the system specification given in the main text. The gain falls well within the bounds described in Sec. 6.

Fig. 5, a state where $\text{GAIN}_c = 1$ means that in this case multiplexing has no advantage over single-source imaging.

Significance of the Model

Suppose we follow the more prevalent methods of demultiplexing and unmixing: treating them as independent processes that are optimized separately. What would the consequences be? Let us ignore here \mathbf{X} during the optimization of \mathbf{W} , i.e., we use Eq. (6) irrespective of \mathbf{X} . The optimized $\widehat{\mathbf{W}}_i$ demultiplexes \mathbf{i} using Eq. (3). Finally, $\widehat{\mathbf{W}}_i$ is used in conjunction with \mathbf{X} for unmixing using Eqs. (8,9). In this case, the estimation error in $\widehat{\mathbf{c}}$ is denoted by $\text{GAIN}_c(\widehat{\mathbf{W}}_i)$. We simulated this on the aforementioned Specimen-I, which is stained with \mathcal{D}_1 . To enable demultiplexing of \mathbf{i} , Case 1 described in Sec. 3 is used, with $N_{\text{measure}} = N_{\text{sources}}$. Fig. 6 compares the results to $\text{GAIN}_c(\widehat{\mathbf{W}}_c)$, which is obtained by our method. Clearly,

$$\text{GAIN}_c(\widehat{\mathbf{W}}_c) > \text{GAIN}_c(\widehat{\mathbf{W}}_i), \quad (24)$$

showing that our approach has a notable advantage over common multiplexing. Moreover, traditional multiplexing may be *harmful*, leading to *net loss* of quality of $\widehat{\mathbf{c}}$, relative to simple single-source imaging. This is seen in Fig. 6, where $\text{GAIN}_c(\widehat{\mathbf{W}}_i) < 1$ in some cases. Running this on other specimens and dyes yielded similar, consistent results.

9. Discussion

The theory described here advances coded and multiplexed sensing by explicitly accounting for natural crosstalk effects. This yields sensing which is tailored to the true underlying elements of interest, and recovers them with quality that is significantly better than the prevailing multiplexing approach (which had excluded consideration of underlying crosstalk). To achieve these results, the paper introduces generalizations of the recovery problem, cost function, gain, and incorporation of differing noise intensities.

Much of the theory is general, beyond fluorescence. We thus believe it can be applied to other multiplexing do-

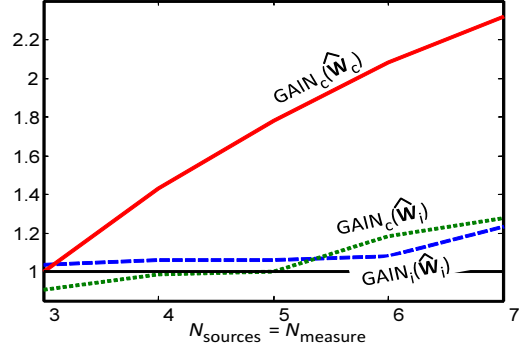


Figure 6. $\text{GAIN}_c(\widehat{\mathbf{W}}_i)$ is achieved by demultiplexing and unmixing using $\widehat{\mathbf{W}}_i$, whose optimization ignored mixing. It is far inferior to GAIN_c obtained using $\widehat{\mathbf{W}}_c$, whose optimization incorporated the mixture model. The former actually decreases the quality of $\widehat{\mathbf{c}}$ when $\text{GAIN}_c(\widehat{\mathbf{W}}_i) < 1$.

ains, in which known cross-talk exists. For example, linear convolution such as blur is expressed as \mathbf{X} in a Töplitz matrix form. The theory has room for further development. *Photobleaching* [19] is a process in which the concentrations $\{c_d\}$ gradually decay over time, in response to the accumulated excitation dosage. Thus, the theory would benefit if the optimization of \mathbf{W} would generalize to account for this effect. Another effect to account for is saturation of the sensor [28], as well as the fluorophores, which can absorb light up to a limit.

A. Estimation of Noise Parameters

The cost function (Eq. 12) depends on the parameters σ_{gray}^2 and $\{\nu_d^2\}_{d=1}^{N_{\text{dyes}}}$, which govern Eq. (14). So does the gradient $\frac{\partial \text{MSE}_c}{\partial \mathbf{W}}$. Thus, these parameters should be calibrated first. Calibrating σ_{gray}^2 is easy since it is independent of the specimen. However, calibrating $\{\nu_d^2\}_{d=1}^{N_{\text{dyes}}}$ is complex. Suppose dye $d = 3$ was the only fluorophore in the specimen. Then ν_3^2 could have been derived (as in [28]), by fitting a straight line to a plot of σ^2 vs. $w_{m,3}^x$. However, exclusive single-dye specimens are irrelevant to our problem. We have at hand a *mixture* of dyes, with unknown concentrations – which this entire paper seeks to estimate.

To make the parameter calibration practical, we approximate Eq. (14) as follows:

$$\sigma_m^2 \approx \sigma_{\text{gray}}^2 + \nu^2 \sum_{d=1}^{N_{\text{dyes}}} w_{m,d}^x. \quad (25)$$

Eq. (25) enables fast calibration for a mixed specimen. The two parameters σ_{gray}^2 and ν^2 are obtained for the entire specimen. This is done by fitting a line to the spatial mean of σ^2 , as a function of $\sum_{d=1}^{N_{\text{dyes}}} w_{m,d}^x$. Simulations showed that the approximation in Eq. (25) is reasonable.

Acknowledgments

We thank the reviewers for their useful comments. Yoav Schechner is a Landau Fellow – supported by the Taub

Foundation, and an Alon Fellow. This work was supported by the Israeli Ministry of Science, Culture and Sport (Grant 3-3426) and the US-Israel Binational Science Foundation (BSF) Grant 2006384. It was conducted in the Ollendorff Minerva Center. Minerva is funded through the BMBF.

References

- [1] A. Agrawal and R. Raskar. Optimal single image capture for motion deblurring. In *Proc. IEEE CVPR*, 2009.
- [2] M. Alterman and Y. Y. Schechner. Minimization of multiplexed unmixing error using gradient descent. *CCIT Report 760, EE Pub No. 1717*, 2010.
- [3] M. Ben-Ezra, J. Wang, B. Wilburn, X. Li, and L. Ma. An led-only BRDF measurement device. In *IEEE CVPR*, 2008.
- [4] D. P. Bertsekas. *Nonlinear Programming*. Athena, 1999.
- [5] O. G. Cula, K. J. Dana, D. K. Pai, and D. Wang. Polarization multiplexing for bidirectional imaging. In *Proc. IEEE CVPR Vol. 2*, pages 1116–1123, 2005.
- [6] M. W. Davidson. Fundamentals of light-emitting diodes (LEDs). In *Education in Microscopy and Digital Imaging*, <http://zeiss-campus.magnet.fsu.edu/>.
- [7] Y. C. Eldar and A. V. Oppenheim. Covariance shaping least-squares estimation. In *IEEE Trans. SP*, 51:686–697, 2003.
- [8] D. Fuhrmann, C. Preza, J. O’Sullivan, D. Snyder, and W. Smith. Spectrum estimation from quantum-limited interferograms. *IEEE Trans. SP*, 52:950–961, 2004.
- [9] Y. Garini, A. Gil, I. Bar-Am, D. Cabib, and N. Katzir. Signal to noise analysis of multiple color fluorescence imaging microscopy. *Cytometry*, 35:214–226, 1999.
- [10] M. E. Gehm, R. John, D. J. Brady, R. M. Willett and T. J. Schulz. Single-shot compressive spectral imaging with a dual-disperser architecture. In *Opt. Express*, 15:14013–14027, 2007.
- [11] M. Harwit and N. J. A. Sloane. *Hadamard Transform Optics*. Academic Press, New York, 1979.
- [12] M. B. Hullin, M. Fuchs, I. Ihrke, H. P. Seidel, and H. P. A. Lensch. Fluorescent immersion range scanning. *ACM TOG*, 27:1–10, 2008.
- [13] S. Ioué and K. R. Spring. *Video Microscopy*, 2nd ed., ch. 6,7,8, Plenum Press, New York, 1997.
- [14] K. C. Lee, J. Ho, and D. J. Kriegman. Acquiring linear subspaces for face recognition under variable lighting. *IEEE Trans. PAMI*, 27:684–698, 2005.
- [15] M. Levoy, B. Chen, V. Vaish, M. Horowitz, I. McDowall, and M. Bolas. Synthetic aperture confocal imaging. *ACM TOG*, 23:825–834, 2004.
- [16] C. K. Liang, T. H. Lin, B.-Y. Wong, C. Liu, and H. H. Chen. Programmable aperture photography: multiplexed light field acquisition. In *ACM TOG*, pages 1–10. ACM, 2008.
- [17] Q. T. Luong, P. Fua, and Y. Leclerc. Recovery of reflectances and varying illuminants from multiple views. In *Proc. ECCV Vol. 3*, pages 163–179, 2002.
- [18] G. McNamara, A. Gupta, J. Reynaert, T. D. Coates, and C. Boswell. Spectral imaging microscopy web sites and data. *Cytometry*, 69A:863–871, 2006.
- [19] F. A. Merchant and A. Periasamy. Fluorescence imaging. In *Microscope Image Processing*. Ch. 12, Elsevier, 2008.
- [20] N. J. W. Morris and K. N. Kutulakos. Reconstructing the surface of inhomogeneous transparent scenes by scatter-trace photography. In *Proc. IEEE ICCV*, 2007.
- [21] A. Mortensen, S. Dyer, R. Hammaker, and W. Fateley. A hadamard-multiplexed spectrometer based on an acousto-optic tunable filter. *IEEE Trans. IM.*, 45:394–398, 1996.
- [22] S. Narasimhan, S. Koppal, and S. Yamazaki. Temporal dithering of illumination for fast active vision. In *Proc. ECCV*, 830–844, 2008.
- [23] R. A. Neher, M. Mitkovski, F. Kirchhoff, E. Neher, F. J. Theis, A. Zeug. Blind source separation techniques for the decomposition of multiply labeled fluorescence images. In *Biophysical Journal*, 9:3791–3800, 2009.
- [24] M. A. Neifeld and P. Shankar. Feature-specific imaging. In *Appl. Opt.*, 42:3379–3389, 2003.
- [25] J. Park, M. Lee, M. D. Grossberg, and S. K. Nayar. Multispectral imaging using multiplexed illumination. In *Proc. IEEE ICCV*, 2007.
- [26] W. S. Rasband. ImageJ, U. S. National Inst. of Health, Bethesda, MD, <http://rsb.info.nih.gov/ij/>, 1997–2009.
- [27] R. Raskar, A. Agrawal, and J. Tumblin. Coded exposure photography: motion deblurring using fluttered shutter. In *ACM TOG*, 795–804, 2006.
- [28] N. Ratner and Y. Y. Schechner. Illumination multiplexing within fundamental limits. In *Proc. IEEE CVPR*, 2007.
- [29] N. Ratner, Y. Y. Schechner and F. Goldberg. Optimal multiplexed sensing: bounds, conditions and a graph theory link. *Opt. Express* 15:17072–17092, 2007.
- [30] I. Sato, T. Okabe, Y. Sato, and K. Ikeuchi. Using extended light sources for modeling object appearance under varying illumination. *Proc. IEEE ICCV*, 1:325–332, 2005.
- [31] M. D. Schaeberle, J. F. Turner, and P. J. Treado. Multiplexed acousto-optic tunable filter (AOTF) spectral imaging microscopy. In *Proc. SPIE vol., 2173*, pages 11–20, 1994.
- [32] Y. Y. Schechner, S. K. Nayar, and P. N. Belhumeur. Multiplexing for optimal lighting. *IEEE Trans. PAMI*, 29:1339–1354, 2007.
- [33] P. Sen, B. Chen, G. Garg, S. R. Marschner, M. Horowitz, M. Levoy, and H. P. A. Lensch. Dual photography. *ACM TOG*, 24:745–755, 2005.
- [34] J. Thigpen and S. K. Shah. *Multispectral imaging*. In *Microscope Image Processing*, Ch. 13. Elsevier, 2008.
- [35] C. D. Tran and R. J. Furlan. Spectrofluorometer based on acousto-optics tunable filter for rapid scanning of multicomponent sample analysis. *Anal. Chem.*, 65:1675–1681, 1993.
- [36] T. Treibitz and Y. Y. Schechner. Recovery limits in pointwise degradation. In *Proc. IEEE ICCP*, 2009.
- [37] A. Wenger, A. Gardner, C. Tchou, J. Unger, T. Hawkins, and P. Debevec. Performance relighting and reflectance transformation with time-multiplexed illumination. *ACM TOG*, 24:756–764, 2005.
- [38] A. Wuttig. Optimal transformations for optical multiplex measurements in the presence of photon noise. *Appl. Opt.*, 44:2710–2719, 2005.
- [39] T. Zimmermann. Spectral imaging and linear unmixing in light microscopy. *Advances in Biochemical Engineering/Biotechnology*, 95:245–265, 2005.